



Artificial Chemist: An Autonomous Quantum Dot Synthesis Bot

Robert W. Epps, Michael S. Bowen, Amanda A. Volk, Kameel Abdel-Latif, Suyong Han, Kristofer G. Reyes, Aram Amassian, and Milad Abolhasani*

The optimal synthesis of advanced nanomaterials with numerous reaction parameters, stages, and routes, poses one of the most complex challenges of modern colloidal science, and current strategies often fail to meet the demands of these combinatorially large systems. In response, an Artificial Chemist is presented: the integration of machine-learning-based experiment selection and high-efficiency autonomous flow chemistry. With the self-driving Artificial Chemist, made-to-measure inorganic perovskite quantum dots (QDs) in flow are autonomously synthesized, and their quantum yield and composition polydispersity at target bandgaps, spanning 1.9 to 2.9 eV, are simultaneously tuned. Utilizing the Artificial Chemist, eleven precision-tailored QD synthesis compositions are obtained without any prior knowledge, within 30 h, using less than 210 mL of total starting QD solutions, and without user selection of experiments. Using the knowledge generated from these studies, the Artificial Chemist is pre-trained to use a new batch of precursors and further accelerate the synthetic path discovery of QD compositions, by at least twofold. The knowledge-transfer strategy further enhances the optoelectronic properties of the in-flow synthesized QDs (within the same resources as the no-prior-knowledge experiments) and mitigates the issues of batch-to-batch precursor variability, resulting in QDs averaging within 1 meV from their target peak emission energy.

Metal halide perovskite quantum dots (QDs) have recently emerged as an exciting class of semiconducting materials and hold the potential to outperform conventional I–VI, IV–VI, and III–V semiconductor nanocrystals in QD-based optoelectronic

devices.^[1–5] Despite the substantial improvement in performance of perovskite QDs over the past 5 years,^[6–9] one major obstacle hindering their development is Edisonian (trial and error)-based QD synthesis, discovery, and optimization methods.^[10] Currently, flask-based and combinatorial experimental platforms are used to search over the vast chemical universe (i.e., reaction space) of metal halide perovskite QDs and their synthetic routes for applications in optoelectronic devices. Such strategies often fail to surpass the output of an expertly guided, albeit ad hoc, manual search, resulting in a time- and cost-intensive discovery of the optimal synthetic pathway.^[11] These methods also fail to meet the challenges imposed by batch-to-batch precursor variability, which is prevalent in QD syntheses.^[12] When moving between laboratories, source chemicals, reactors, or even replicates in a QD synthesis, it is difficult to attain a consistent product. Colloidal semiconductor nanocrystals are highly complex and sensitive materials, where two compositionally

identical solutions may have entirely different optoelectronic properties (differently sized nanocrystals). The massive chemical universe of colloidal QDs and strong dependency of their optoelectronic properties on environmental/synthesis conditions demonstrates a need for a high-efficiency autonomous robotic experimentation strategy, located in-house with the synthetic chemist, to rapidly mine the experimentally-obtained QD synthesis data and intelligently select the next reaction conditions.

While in their infancy, self-optimizing devices have begun to unravel the challenges of these more complex chemical processes, with their existing applications spanning organic reactions to nanocrystal syntheses.^[13–15] Recent advances in supervised and reinforcement machine learning (ML) techniques, such as multi-output neural networks (NNs), ensemble methods, and Bayesian optimization, provide an exciting opportunity for reshaping the synthesis and optimization of QDs through the ML-based direction of a high-throughput QD synthesizer.^[16] Among the rapidly growing variety of ML applications, including expedited and enhanced analyses of complex reaction data sets,^[17–19] deep reinforcement learning algorithms have recently been demonstrated to outperform highly trained human experts when utilized to predict the outcome, optimize the yield,

R. W. Epps, M. S. Bowen, A. A. Volk, K. Abdel-Latif, S. Han,
Prof. M. Abolhasani

Department of Chemical and Biomolecular Engineering
North Carolina State University
Raleigh, NC 27606, USA

E-mail: abolhasani@ncsu.edu

Prof. K. G. Reyes
Department of Materials Design and Innovation
University at Buffalo
Buffalo, NY 14260, USA

Prof. A. Amassian
Department of Material Science and Engineering
Organic and Carbon Electronics Laboratories (ORaCEL)
North Carolina State University
Raleigh, NC 27606, USA

 The ORCID identification number(s) for the author(s) of this article can be found under <https://doi.org/10.1002/adma.202001626>.

DOI: 10.1002/adma.202001626

and plan synthesis routes of various reactions in both supervised and self-optimizing systems. Such ML-accelerated strategies have been effectively applied to a large number of studies, which span organic synthesis planning and optimization^[20–24] to the formation of advanced materials, including single-crystal perovskites,^[25] metal–organic frameworks and nanocapsules,^[26,27] gold nanoclusters,^[16] and lead sulfide QDs.^[28] Capitalizing on the recent progress of ML-enhanced optimization algorithms, a smart QD manufacturing strategy that relies on decision-making algorithms and NNs trained on experimentally-measured QD properties can significantly accelerate the synthetic path discovery, optimization, and continuous manufacturing of colloidal QDs with precision-tailored optoelectronic properties.

In this work, we present a smart flow-based QD synthesis strategy (i.e., the Artificial Chemist), which utilizes plug-and-play fluidic microreactors capable of autonomous synthesis and optimization of colloidal QDs across multiple target parameters simultaneously. The Artificial Chemist, shown in **Figure 1**, can rapidly and efficiently: i) explore the vast chemical universe of colloidal QDs, ii) learn the colloidal QD synthesis pathway(s) to achieve specific optoelectronic properties, iv) archive and transfer the in-house generated knowledge to the subsequent synthesis experiments, and v) continuously synthesize the rapidly optimized QDs on-demand, all within a single enclosed system and at a fraction of the time and cost of batch techniques. The plug-and-play intelligent QD synthesis technology utilizes a custom-developed *in situ* UV–Vis absorption (A) and photoluminescence (PL) spectrum monitoring module in conjunction with a real-time ML-based Bayesian optimization algorithm to enable, for the first time, the simultaneous optimization of PL quantum yield (PLQY, Φ) and emission linewidth (E_{FWHM}), of colloidal QDs for any desired peak emission energy (E_p) in the visible range.

Utilizing the developed Artificial Chemist, we studied over 1400 reactions across eleven target E_p values and eight different reaction optimization algorithms. Such smart/modular flow synthesis techniques can be readily adapted for on-demand synthesis, discovery, and optimization of other classes of nanoparticles beyond perovskite QDs (e.g., metal or metal oxide).

Automated experimentation strategies often reduce the cost and time required to study and synthesize materials,^[29] but the dependency on user-driven experiment selection undoubtedly limits their exploration and optimization efficiency. A fully closed-loop autonomous experiment selection and execution platform (i.e., the Artificial Chemist), would therefore, significantly expedite the tedious process of colloidal synthetic path discovery and reaction optimization, at a fraction of the cost and material consumption of the current paradigm. The self-driving Artificial Chemist is comprised of a precursor formulation module (seven syringe pumps, two syringe refill systems, and two inline passive micromixers), a flow reactor module, and an *in situ* QD characterization module (a custom-developed flow cell for simultaneous A and PL monitoring). Flow is segmented into reactive solution and perfluorinated oil (PFO) phases. The PFO carrier phase enhances mass transfer in the reactive phase and minimizes fouling by separating the reactive solution from the tubing wall.^[30] The operation sequence of each colloidal synthesis reaction, including reagent refill, spectral sampling, and real-time processing are fully automated using a central computer controller. To evaluate the performance of the developed Artificial Chemist, we studied the bandgap tuning of metal halide perovskite QDs through halide exchange reactions,^[31–34] using flow-synthesized cesium lead bromide (CsPbBr_3) QDs as the starting quantum dots (SQDs).^[35,36]

Bandgap tuning of perovskite QDs through the halide exchange reactions occurs when the CsPbBr_3 SQDs react with

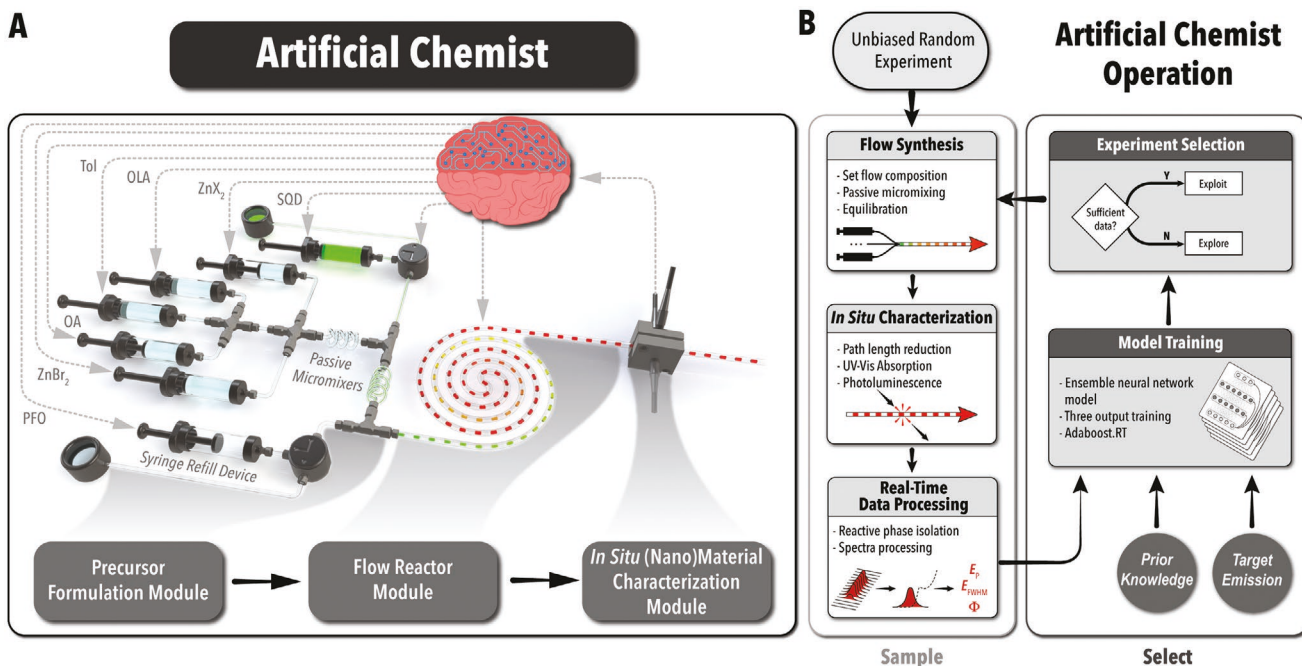


Figure 1. Design and operation of the Artificial Chemist. A) Schematic of the developed smart modular fluidic microprocessor for autonomous synthetic path discovery and optimization of colloidal QDs and B) the process flow diagram detailing its operation.

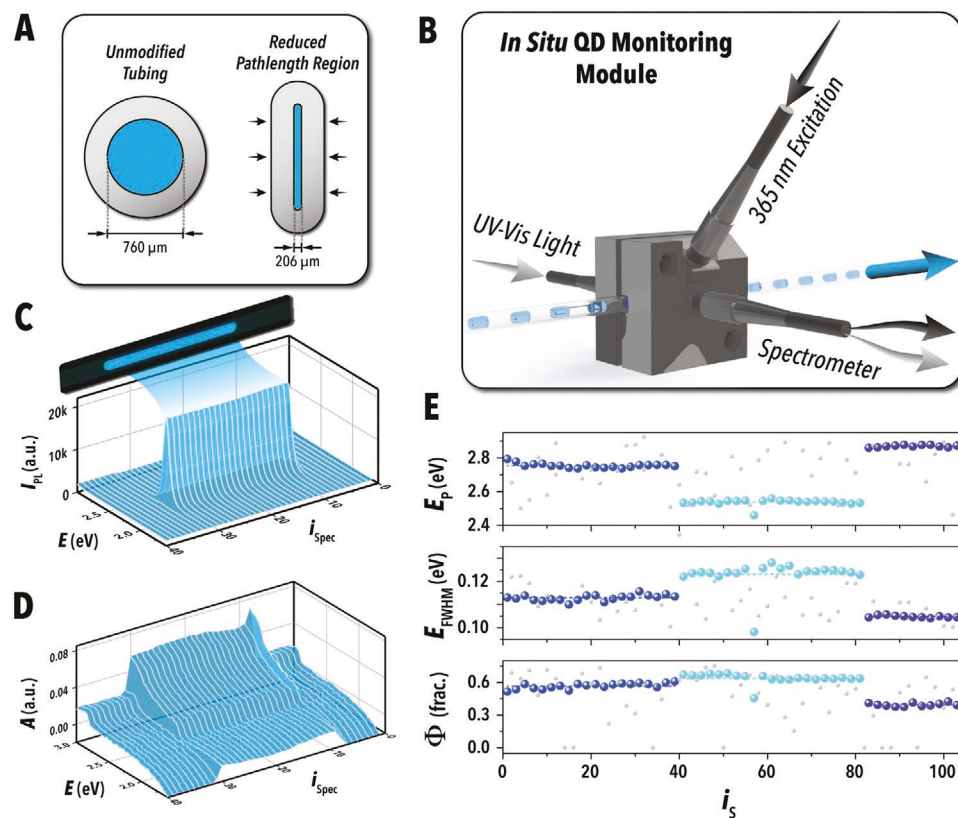


Figure 2. Sampling precision with the reduced path length flow cell. A–D) Illustrations of the compressed tubing cross-section at the sampling location before and after deformation (A) and the fully assembled flow cell (B) with corresponding inline collected photoluminescence (C) and absorption (D) spectra for a single reactive phase slug. E) Demonstration of independent and precise sampling, where three different flow compositions (blue, cyan, and purple) are alternated with randomized experiments (gray).

a mixed zinc halide precursor (zinc iodide [ZnI_2], zinc chloride [ZnCl_2], or zinc bromide [ZnBr_2]) and a specified quantity of oleic acid (OA) and oleylamine (OLA)—represented in their non-dimensional forms as X_{SQD} , X_{ZnX_2} , X_{ZnBr_2} , X_{OA} , and X_{OLA} (see S3, Supporting Information). The developed Artificial Chemist is integrated with a central control system comprising an array of adaptive sampling algorithms, including an ensemble neural network (NNE)-based Bayesian optimization algorithm with an intelligent decision-making policy. The control system (Figure 1B) alternates between controlling the autonomous flow reactor with in situ QD sampling and selecting the next best set of reaction conditions based on the constantly updated NNE model and the decision-making policy.

While it is often overlooked in in situ studies of colloidal QDs, quantification of PLQY is a vital component in predicting the potential performance of as-synthesized QD samples in targeted optoelectronic device applications, such as solar cells and light emitting diodes.^[37] Yet to date, accurate in situ measurement of PLQY has not been possible without substantial dilution of the reactive phase. The Artificial Chemist overcomes this key bottleneck with the help of a novel reduced path length (≈ 0.2 mm) flow cell. This innovation allows us to achieve unprecedented accuracy for in situ PLQY measurements of high concentration QD samples synthesized in flow without disturbing flow uniformity. Utilizing this QD monitoring module, illustrated

in Figure 2A,B, the PLQY of in-flow synthesized perovskite QDs is measured in situ and analyzed in real-time without dilution of the reactive phase, as further detailed in Figure S1, Supporting Information. The spectral monitoring module thus enables accurate in situ optical characterization of colloidal QDs at realistic synthetic conditions and concentrations for QDs deployed in optoelectronic devices.^[38] The real-time processing of in situ obtained A/PL spectra of halide-exchanged perovskite QDs (Figure 2C,D) enables rapid, precise, and order-independent measurements of E_p , E_{FWHM} , and PLQY. Figure 2E and Figures S2 and S3, Supporting Information, illustrate the robustness and reproducibility of the developed Artificial Chemist in its ability to sample specific QD compositions for three specified input conditions, even when the experiments are partitioned by randomly selected synthetic conditions.

At the start of any experimentation, reaction space modeling algorithms may be applied using either no prior training—that is, uninformed—or pre-trained with a limited archived experimental data set. Beginning a synthesis with prior training usually expedites convergence to optimal reaction conditions; however, the required training data is often unavailable for the specific reaction, incomplete, and/or simply not sufficiently consistent across research groups or synthesis platforms to apply with confidence. This is a common challenge in synthetic chemistry and one the Artificial Chemist must be able to overcome. To do so, we compare variations of an NNE approach to

other commonly used algorithms within a black box optimization environment, including “stable noisy optimization by branch and fit” (SNOBFIT)^[39] and “covariance matrix adaptation evolution strategy” (CMA-ES).^[40,41] We apply this optimization method in a transfer learning system, that is, utilizing archived experimental data sets with a new batch of precursors to form higher quality QDs. This strategy encompasses the optimization of the reaction conditions for the target colloidal QDs as well as the mitigation of batch-to-batch precursor variation in current state-of-the-art manufacturing strategies. Full input-output profiles of all studied algorithms are included in Figure S4, Supporting Information.

Effective reaction optimization relies on a belief model that accurately predicts outcomes and their uncertainty and a decision-making policy that efficiently navigates the model space. Many prior studies have applied Gaussian processes (GPs) to model these predictions and uncertainty estimates.^[10,42,43] However, it is difficult to impose complex structure on the GPs, which often simply encode continuity, smoothness, or periodicity. While many reaction systems are effectively modeled under these assumptions,^[44] this limitation inhibits GPs’ ability to sufficiently represent certain reaction spaces, including the complex space explored in this study (Figure 3A,B). Subsequently, we found GPs to underperform in our system when

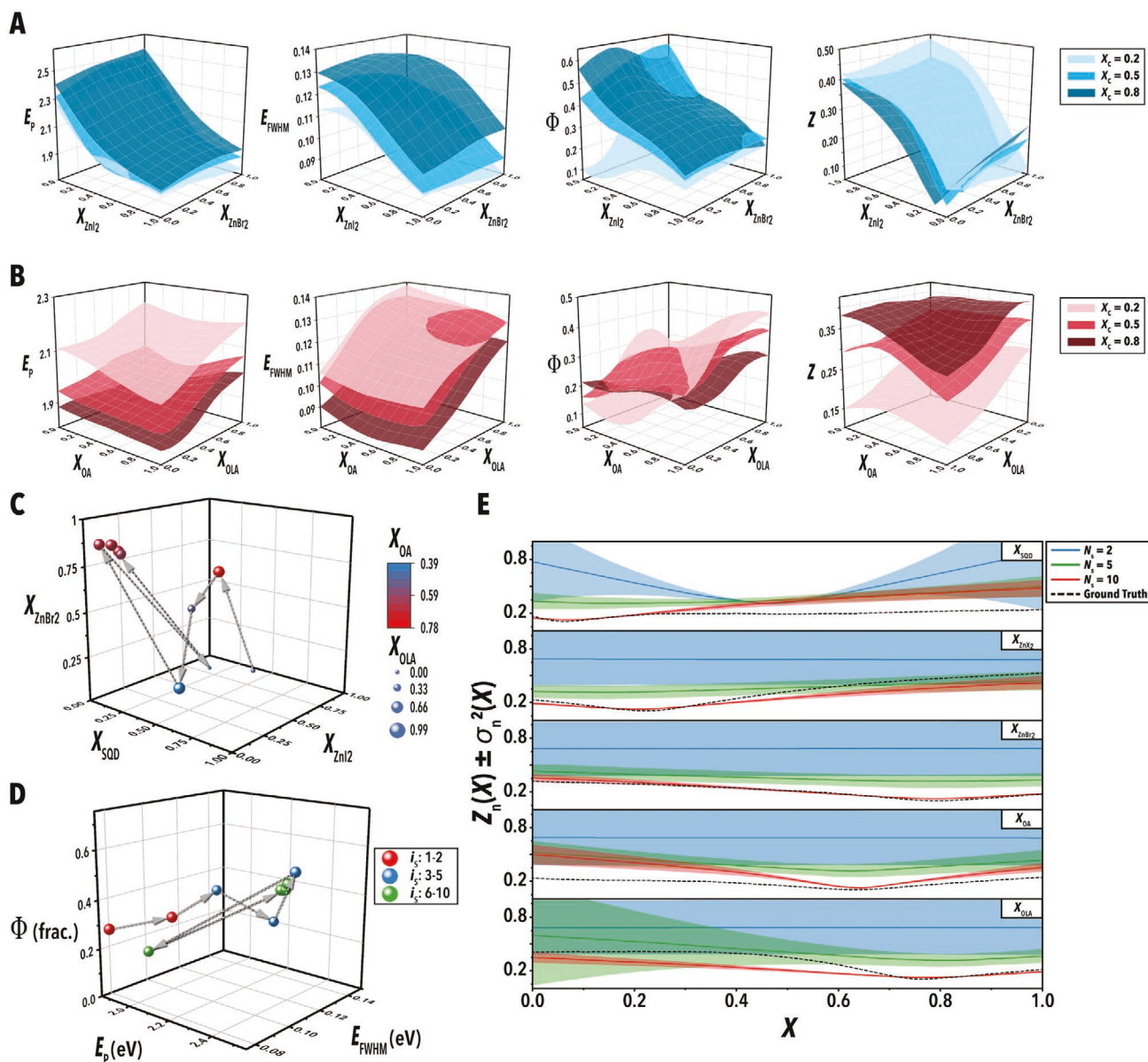


Figure 3. The chemical universe exploration of the Artificial Chemist. A,B) Average model outputs when trained on 150 samples as a function of X_{ZnI_2} and X_{ZnBr_2} (A) and X_{OA} and X_{OLA} (B) when all remaining input variables are kept at a constant value (X_c). C) Input parameter space for ten condition sample set and D) corresponding output parameters used for model training where sampling order is indicated by the direction of the arrows. E) Model prediction average (Z_n) with associated variance (σ^2) as a function of sample size and input parameter at the measured optimal condition for 2.3 eV setpoint emission (i.e., the panels show the predicted Z for each parameter while the remaining parameters are held at their optimal value).

compared with other methods (Figure S4H, Supporting Information). To overcome these issues without losing the statistical quantification that GPs provide, we trained an NNE simultaneously for E_p , E_{FWHM} , and PLQY figures of merit (shown in Figure 3C–E). Sample statistics calculated from the ensemble can then be used in place of the probabilistic quantification traditionally modeled by GPs. The model outputs of these three parameters are converted into a single quality metric-referenced as the objective function (Z). Demonstrated in Figure S5, Supporting Information, we further enhanced the ensemble modeling by applying a data and model boosting algorithm, Ada-boost,^[45,46] to train models in the ensemble. Ada-boost assigns data weights iteratively between successively trained NNs as well as a model weight to each individual NN, thereby increasing the influence of higher performing members of the ensemble. Finally, a decision policy selected from four different methods was used on the boosted NNE model to choose the next set of optimized experimental conditions for a targeted QD bandgap.

Across different decision policies applied to the NNE model of the Artificial Chemist, a balance between exploration of the chemical space and exploitation of the best predicted regions of the reaction space—shown in Figure 4A—resulted in the lowest number of experiments (cost) required to achieve the desired optoelectronic

properties of metal halide perovskite QDs.^[47] Exploration-heavy optimization strategies such as NNE with maximum variance (MV) and SNOBFIT, all either failed to consistently move inwards from the input space bounds or converged onto an optimum synthetic condition at a far slower rate than other models. On the opposite end of this balance, NNE with pure exploitation (EPLT) also failed to converge onto an optimum within an acceptable number of experiments (less than 25), due to the small incremental improvements with each round of experimentation. The colloidal synthesis optimization methods with more balanced exploration/exploitation—for example, NNE with upper confidence bound (UCB), NNE with expected improvement (EI), and CMA-ES—rapidly and consistently reached the optimal synthesis conditions (see Figure 4B and Figure S6, Supporting Information). All three of these methods on average resulted in QDs within 10% of the lowest measured Z value after 25 experiments. Among the balanced exploration/exploitation methods tested here and represented in Figure 4C, NNE-UCB showed the most consistent and greatest performance in the uninformed QD synthesis environment.

A noteworthy advantage of the objective function optimization method over multi-parameter optimization techniques^[48] is that it may easily be adapted towards precise bandgap selection, specifically after uninformed synthetic path discovery has taken

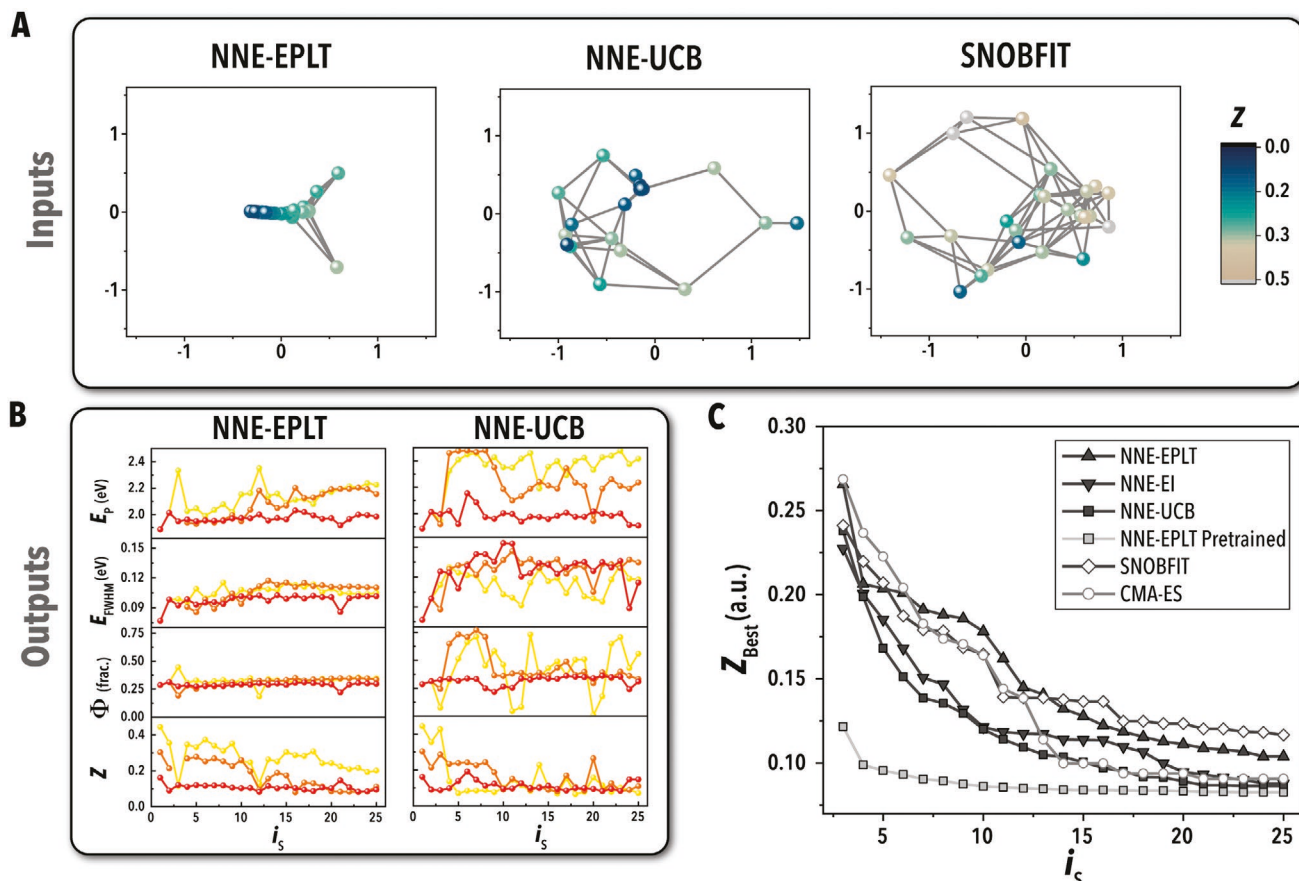


Figure 4. Intelligent decision-making of the Artificial Chemist. A) Isomap representation of the input space for a target emission of 2.2 eV across three different optimization methods ranging in exploration to exploitation ratios. NNE-EPLT: exploitation-heavy; NNE-UCB: balanced exploration versus exploitation; SNOBFIT: exploration-heavy. B) Sample output values for NNE-UCB and NNE-EPLT (yellow, orange, and red corresponding to 2.4, 2.2, and 2.0 eV, respectively). C) Mean of best three measured Z , averaged across six optimizations of different target emissions, as a function of sample number.

place (knowledge transfer). In addition to the optimization runs performed without any prior information on the reaction space of metal halide perovskite QDs, we explored the pre-training of NNE models with prior optimization data sets to both further push the limits of the objective function multi-parameter optima (i.e., Pareto front) and to accommodate batch-to-batch precursor variability in the starting reagents. An NNE model was trained with the data collected for the NNE-UCB optimizations (275 experiments) then passed through an EPLT policy. Despite the perovskite QD synthesis occurring with a new set of precursors, the pre-trained optimization surpassed the performance of all other methods for 9 of the 11 target E_p values (5 with ZnI_2 and 4 with ZnCl_2). Optimal conditions for the two exceptions (1.9 and 2.5 eV) were collected during the uninformed NNE-UCB study and were located near the bounds of the available

reaction space for each of the halides. After 25 runs, autonomously synthesized perovskite QDs with prior knowledge had E_p values, on average, within 1 meV of the target values, which is an improvement from the 3 meV of the uninformed NNE-UCB experiments. Thus, the developed Artificial Chemist can rapidly and consistently find the optimal synthetic pathway of QDs using the knowledge obtained from prior experiments even when prior data is subject to batch-to-batch precursor variation.

The Artificial Chemist is capable of rapidly reaching favorable synthesis conditions for a desired set of optoelectronic properties of QDs with no prior reaction space data. Furthermore, it is able to use prior training to push the measured figures of merit (i.e., E_p , E_{FWHM} , and PLQY) past the reported results of less efficient methods within the same resources (as shown in Figure 5A,B). The approach of using NNE-UCB optimization followed by

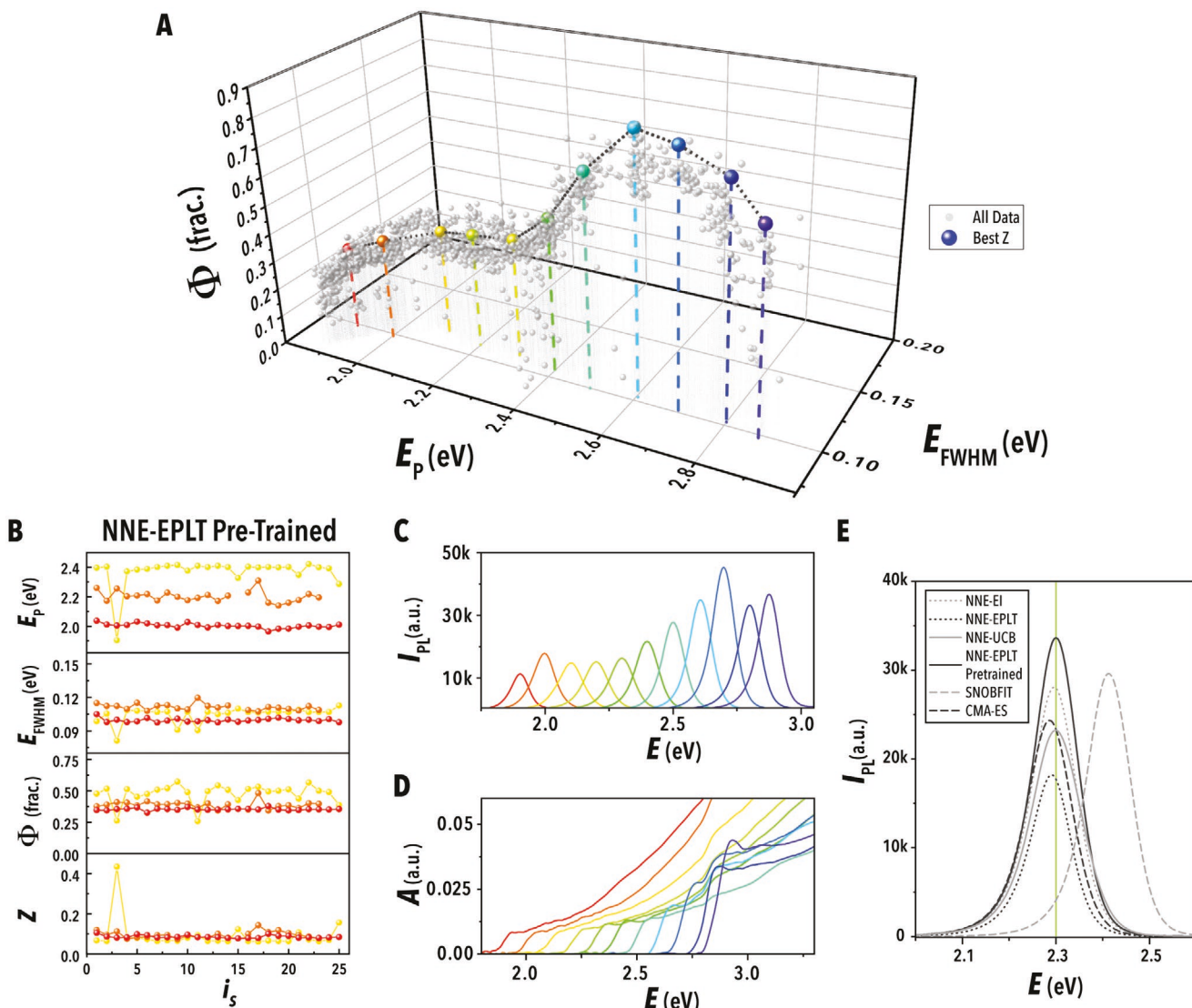


Figure 5. Case study of the Artificial Chemist in the accelerated synthesis of metal halide perovskite QDs. A) PLQY as a function of E_p and E_{FWHM} for all 1400 in-flow collected data points with the 11 optimal formulations highlighted. B) Sample output values for a pre-trained NNE-EPLT at three separate target emission values (yellow, orange, and red correspond to 2.4, 2.2, and 2.0 eV respectively). C) In situ photoluminescence and D) absorption spectra of 11 optimized nanocrystals, linearly scaled by the concentration of SQD in the reactive phase. E) PL spectra, scaled by the measured absorbance at 365 nm, of best measured Z for six sample selection methods.

pre-trained NNE-EPLT was able to produce high-quality metal halide perovskite QDs all within, on average, 1 meV of targeted E_p values (Figure 5C,D). These methods demonstrated significant improvements over all optimization strategies and decision policies evaluated in this study (Figure 5E). Further applications of the Artificial Chemist will enable facile manufacturing of made-to-measure colloidal nanocrystals with precise synthesis control across different precursor batches. Archived experimental results facilitate rapid tuning of reaction parameters to achieve consistent nanocrystal batches and optoelectronic properties in a continuous flow production setting.

The Artificial Chemist, in addition to accelerated synthetic path discovery and optimization of colloidal QDs, can also rapidly synthesize a library of high-quality QDs on-demand, as shown in Figure 6A,B, utilizing the NNE-EPLT optimization algorithm with pre-training based on in-house generated QD synthesis data. That is, through knowledge transfer of prior experimental data sets, the Artificial Chemist can quickly attain high PLQY and low polydispersity (E_{FWHM}) QDs for any targeted emission color. The autonomously discovered optimal synthetic pathways (QD formulations) by the Artificial Chemist may then be utilized for a scaled-up (nano)manufacturing of the target perovskite QDs by continuously flowing reactants through the same modular flow synthesis platform with a throughput of ≈ 220 g QD solids per day (Figure 6C).

In this work, we have developed the self-driving Artificial Chemist, that is, a single, self-contained system capable of autonomous data generation, learning, synthetic path discovery,

knowledge transfer, and continuous on-demand manufacturing of solution-processed nanomaterials. We have integrated ML-based experimental selection methods with a high-efficiency modular fluidic reactor to demonstrate a system capable of fully autonomous and intelligent materials chemistry exploration, as well as efficient multivariate process optimization with knowledge transfer. We attained accurate *in situ* characterization of PLQY, E_{FWHM} , and E_p of in-flow synthesized QDs. Our methods enabled the simultaneous optimization of three important, highly coupled parameters for QD quality and identified the synthetic routes to achieving the frontier properties of these materials. With this approach, we studied the efficacy of NNE modeling in the uninformed optimization of the halide exchange of CsPbBr_3 QDs. By applying knowledge transfer from the uninformed studies, the intelligent system was then utilized to produce high-quality metal halide perovskite QDs within 1 meV of 11 target peak emission energies.

The developed plug-and-play autonomous flow synthesis strategy may be quickly adapted to other reaction systems beyond colloidal QDs such as metal, metal oxide, and carbon-based nanoparticles. This approach can also be expanded to include downstream dispensing of colloidal suspensions and solutions directly into coating and printing platforms for the fabrication of optoelectronic devices. An additional implication of the Artificial Chemist is intensified, green, and more consistent manufacturing of advanced nanomaterials as compared to flask-based studies, which are limited by batch-to-batch precursor variations and inefficient/irreproducible heat and mass transfer rates. The

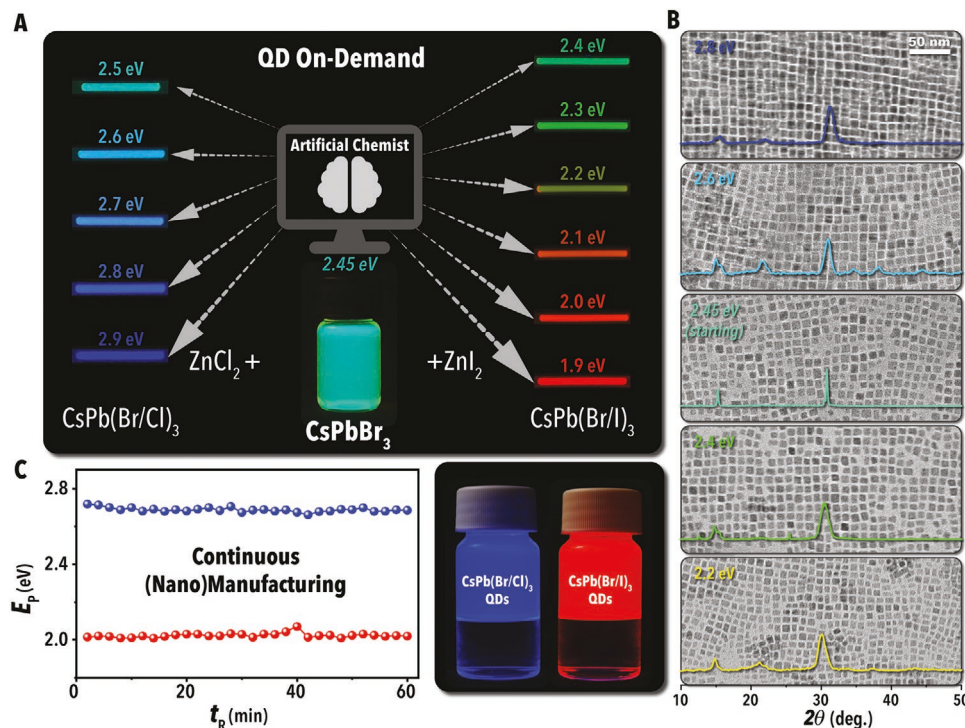


Figure 6. QD synthesis on-demand enabled by the Artificial Chemist. A) Illustration of the UV-illuminated starting perovskite QDs and final halide-exchanged synthesized in flow for all 11 target emission colors. B) Transmission electron microscopy (TEM) images with X-ray diffraction (XRD) spectra overlay of the purified halide-exchanged QDs obtained from (descending order) ZnCl_2 exchange reactions with target emissions of 2.8 and 2.6 eV, the starting QDs, and ZnI_2 reactions with target emissions of 2.4 and 2.2 eV. C) E_p values continuously measured for a 1 h continuous collection of 2.7 eV (blue) and 2.0 eV (red) perovskite QDs with the corresponding UV illuminated products in 20 mL vials.

autonomous robotic experimentation strategy embodied by the Artificial Chemist offers broad-reaching applications in rapidly advancing the synthesis of colloidal semiconductor nanocrystals and any other solution-processed nanomaterial.

Supporting Information

Supporting Information is available from the Wiley Online Library or from the author.

Acknowledgements

The authors gratefully acknowledge the financial support provided by the National Science Foundation (Award # 1902702), the UNC Research Opportunities Initiative program, and North Carolina State University. This work was performed in part at the Analytical Instrumentation Facility (AIF) at North Carolina State University, which is supported by the State of North Carolina and the National Science Foundation (award number ECCS-1542015). The AIF is a member of the North Carolina Research Triangle Nanotechnology Network (RTNN), a site in the National Nanotechnology Coordinated Infrastructure (NNCI). All data used in this study is available upon request.

Conflict of Interest

The authors declare no conflict of interest.

Author Contributions

M.A. conceived the Artificial Chemist idea, designed the project, and coordinated the efforts of the research team. R.W.E and M.A. designed the microfluidic flow reactor, including the reduced path length flow cell, and drafted the manuscript. R.W.E programmed the automated flow, data processing, and neural network-based modeling systems; conducted all flow experiments; and performed the offline flow data processing. M.S.B. and R.W.E. developed preliminary halide exchange studies, performed preliminary neural network-based model selection, and integrated the machine learning algorithms with the flow controller. A.A.V. conducted all XRD and GIXRD measurements and reduced path length flow cell measurement validations. A.A. and A.A.V. analyzed the XRD and GIXRD data. K.A. developed the starting QD synthesis protocol and conducted all TEM imaging. S.H. designed and compiled the video time-lapse study. K.G.R., R.W.E, and M.A. designed the machine-learning optimization architecture. K.G.R. designed and programmed the decision-making policies. All authors reviewed the manuscript and provided relevant feedback.

Keywords

autonomous synthesis, machine learning, microfluidics, perovskites, quantum dots

Received: March 7, 2020

Revised: April 7, 2020

Published online:

[1] E. H. Sargent, *Nat. Photonics* **2012**, *6*, 133.

[2] K.-S. Cho, E. K. Lee, W.-J. Joo, E. Jang, T.-H. Kim, S. J. Lee, S.-J. Kwon, J. Y. Han, B.-K. Kim, B. L. Choi, J. M. Kim, *Nat. Photonics* **2009**, *3*, 341.

- [3] S. Wang, Y. Wang, Y. Zhang, X. Zhang, X. Shen, X. Zhuang, P. Lu, W. W. Yu, S. V. Kershaw, A. L. Rogach, *J. Phys. Chem. Lett.* **2019**, *10*, 90.
- [4] X. Zhang, X. Bai, H. Wu, X. Zhang, C. Sun, Y. Zhang, W. Zhang, W. Zheng, W. W. Yu, A. L. Rogach, *Angew. Chem., Int. Ed.* **2018**, *57*, 3337.
- [5] R. Azmi, S. Sinaga, H. Aqoma, G. Seo, T. K. Ahn, M. Park, S.-Y. Ju, J.-W. Lee, T.-W. Kim, S.-H. Oh, S.-Y. Jang, *Nano Energy* **2017**, *39*, 86.
- [6] Q. A. Akkerman, G. Rainò, M. V. Kovalenko, L. Manna, *Nat. Mater.* **2018**, *17*, 394.
- [7] Y. Nagaoka, K. Hills-Kimball, R. Tan, R. Li, Z. Wang, O. Chen, *Adv. Mater.* **2017**, *29*, 1606666.
- [8] N. Chen, T. Cai, W. Li, K. Hills-Kimball, H. Yang, M. Que, Y. Nagaoka, Z. Liu, D. Yang, A. Dong, C.-Y. Xu, R. Zia, O. Chen, *ACS Appl. Mater. Interfaces* **2019**, *11*, 16855.
- [9] L. Protesescu, S. Yakunin, M. I. Bodnarchuk, F. Krieg, R. Caputo, C. H. Hendon, R. X. Yang, A. Walsh, M. V. Kovalenko, *Nano Lett.* **2015**, *15*, 3692.
- [10] L. Bezingé, R. M. Maceczky, I. Lignos, M. V. Kovalenko, A. J. deMello, *ACS Appl. Mater. Interfaces* **2018**, *10*, 18869.
- [11] A. Vikram, V. Kumar, U. Ramesh, K. Balakrishnan, N. Oh, K. Deshpande, T. Ewers, P. Trefonas, M. Shim, P. J. A. Kenis, *Chem. Nano. Mat.* **2018**, *4*, 943.
- [12] A. M. Nightingale, J. C. de Mello, *J. Mater. Chem.* **2010**, *20*, 8454.
- [13] D. E. Fitzpatrick, C. Battilocchio, S. V. Ley, *Org. Process Res. Dev.* **2016**, *20*, 386.
- [14] S. Krishnadasan, R. J. C. Brown, A. J. deMello, J. C. deMello, *Lab Chip* **2007**, *7*, 1434.
- [15] C. Mateos, M. J. Nieves-Remacha, J. A. Rincón, *React. Chem. Eng.* **2019**, *4*, 1536.
- [16] J. Li, T. Chen, K. Lim, L. Chen, S. A. Khan, J. Xie, X. Wang, *Adv. Intell. Syst.* **2019**, *1*, 1900029.
- [17] H. Wang, Y. Xie, D. Li, H. Deng, Y. Zhao, M. Xin, J. Lin, *J. Chem. Inf. Model.* **2020**, *60*, 2004.
- [18] Z. Huang, S. Siddhanta, G. Zheng, T. Kickler, I. Barman, *Angew. Chem., Int. Ed.* **2020**, *59*, 5972.
- [19] J. L. Lansford, D. G. Vlachos, *Nat. Commun.* **2020**, *11*, 1513.
- [20] J. M. Granda, L. Donina, V. Dragone, D.-L. Long, L. Cronin, *Nature* **2018**, *559*, 377.
- [21] S. Steiner, J. Wolf, S. Glatzel, A. Andreou, J. M. Granda, G. Keenan, T. Hinkley, G. Aragon-Camarasa, P. J. Kitson, D. Angelone, L. Cronin, *Science* **2019**, *363*, eaav2211.
- [22] C. W. Coley, D. A. Thomas, J. A. M. Lummiss, J. N. Jaworski, C. P. Breen, V. Schultz, T. Hart, J. S. Fishman, L. Rogers, H. Gao, R. W. Hicklin, P. P. Plehiers, J. Byington, J. S. Piotti, W. H. Green, A. J. Hart, T. F. Jamison, K. F. Jensen, *Science* **2019**, *365*, eaax1566.
- [23] C. W. Coley, W. Jin, L. Rogers, T. F. Jamison, T. S. Jaakkola, W. H. Green, R. Barzilay, K. F. Jensen, *Chem. Sci.* **2019**, *10*, 370.
- [24] Z. Zhou, X. Li, R. N. Zare, *ACS Cent. Sci.* **2017**, *3*, 1337.
- [25] J. Kirman, A. Johnston, D. A. Kuntz, M. Askerka, Y. Gao, P. Todorović, D. Ma, G. G. Privé, E. H. Sargent, *Matter* **2020**, *2*, 938.
- [26] S. M. Moosavi, A. Chidambaram, L. Talirz, M. Haranczyk, K. C. Stylianou, B. Smit, *Nat. Commun.* **2019**, *10*, 539.
- [27] Y. Xie, C. Zhang, X. Hu, C. Zhang, S. P. Kelley, J. L. Atwood, J. Lin, *J. Am. Chem. Soc.* **2020**, *142*, 1475.
- [28] O. Vozny, L. Levina, J. Z. Fan, M. Askerka, A. Jain, M.-J. Choi, O. Ouellette, P. Todorović, L. K. Sagar, E. H. Sargent, *ACS Nano* **2019**, *13*, 11122.
- [29] B. K. H. Yen, A. Günther, M. A. Schmidt, K. F. Jensen, M. G. Bawendi, *Angew. Chem., Int. Ed.* **2005**, *44*, 5447.
- [30] K. S. Elvira, X. C. i. Solvas, R. C. R. Wootton, A. J. deMello, *Nat. Chem.* **2013**, *5*, 905.
- [31] T. Zhang, G. Li, Y. Chang, X. Wang, B. Zhang, H. Mou, Y. Jiang, *CrystEngComm* **2017**, *19*, 1165.

[32] K. Abdel-Latif, R. W. Epps, C. B. Kerr, C. M. Papa, F. N. Castellano, M. Abolhasani, *Adv. Funct. Mater.* **2019**, *29*, 1900712.

[33] G. Nedelcu, L. Protesescu, S. Yakunin, M. I. Bodnarchuk, M. J. Grotevent, M. V. Kovalenko, *Nano Lett.* **2015**, *15*, 5635.

[34] D. Zhang, Y. Yang, Y. Bekenstein, Y. Yu, N. A. Gibson, A. B. Wong, S. W. Eaton, N. Kornienko, Q. Kong, M. Lai, A. P. Alivisatos, S. R. Leone, P. Yang, *J. Am. Chem. Soc.* **2016**, *138*, 7236.

[35] S. Wei, Y. Yang, X. Kang, L. Wang, L. Huang, D. Pan, *Chem. Commun.* **2016**, *52*, 7265.

[36] R. W. Epps, K. C. Felton, C. W. Coley, M. Abolhasani, *Lab Chip* **2017**, *17*, 4040.

[37] D. A. Hanifi, N. D. Bronstein, B. A. Koscher, Z. Nett, J. K. Swabeck, K. Takano, A. M. Schwartzberg, L. Maserati, K. Vandewal, Y. van de Burgt, A. Salleo, A. P. Alivisatos, *Science* **2019**, *363*, 1199.

[38] X. Ling, S. Zhou, J. Yuan, J. Shi, Y. Qian, B. W. Larson, Q. Zhao, C. Qin, F. Li, G. Shi, C. Stewart, J. Hu, X. Zhang, J. M. Luther, S. Duhm, W. Ma, *Adv. Energy Mater.* **2019**, *9*, 1900721.

[39] W. Huyer, A. Neumaier, *ACM T. Math. Software* **2008**, *35*, 1.

[40] N. Hansen, A. Ostermeier, *Evol. Comput.* **2001**, *9*, 159.

[41] N. Hansen, A. Ostermeier, in *Proc. of IEEE Int. Conf. on Evolutionary Computation*, IEEE, Piscataway, NJ, USA **1996**, pp. 312–317.

[42] R. M. Maceiczyk, A. J. deMello, *J. Phys. Chem. C* **2014**, *118*, 20026.

[43] M. A. Osborne, R. Garnett, S. J. Roberts, *Gaussian Processes for Global Optimization* **2009**, Available from: <http://www.robots.ox.ac.uk/~parg/pubs/OsborneGarnettRobertsGPGO.pdf> (accessed: May 2020).

[44] K. M. Tibbetts, X.-J. Feng, H. Rabitz, *Phys. Chem. Chem. Phys.* **2017**, *19*, 4266.

[45] Y. Freund, R. E. Schapire, *JSAI* **1999**, *14*, 771.

[46] D. P. Solomatine, D. L. Shrestha, in *IEEE Int. Joint Conf. on Neural Networks*, IEEE, Piscataway, NJ, USA **2004**, pp. 1163–1168.

[47] W. G. Macready, D. H. Wolpert, *IEEE Trans. Evol. Comput.* **1998**, *2*, 2.

[48] A. M. Schweidtmann, A. D. Clayton, N. Holmes, E. Bradford, R. A. Bourne, A. A. Lapkin, *Chem. Eng. J.* **2018**, *352*, 277.